Mechanical Systems and Signal Processing ▮ (▮▮▮▮) ▮▮▮–▮▮▮

Contents lists available at ScienceDirect

Mechanical Systems and Signal Processing

journal homepage: www.elsevier.com/locate/ymssp

Distributed model-based nonlinear sensor fault diagnosis in wireless sensor networks

Chun Lo [a], Jerome P. Lynch [a,b,*], Mingyan Liu [a]

[a] Electrical Engineering and Computer Science, University of Michigan, Ann Arbor, USA
[b] Civil and Environmental Engineering, University of Michigan, Ann Arbor, USA

ARTICLE INFO

Article history:
Received 14 May 2014
Received in revised form
27 February 2015
Accepted 10 May 2015

Keywords:
Wireless sensor networks
Fault detection
Non-linearity
Distributed systems

ABSTRACT

Wireless sensors operating in harsh environments have the potential to be error-prone. This paper presents a distributive model-based diagnosis algorithm that identifies non-linear sensor faults. The diagnosis algorithm has advantages over existing fault diagnosis methods such as centralized model-based and distributive model-free methods. An algorithm is presented for detecting common non-linearity faults without using reference sensors. The study introduces a model-based fault diagnosis framework that is implemented within a pair of wireless sensors. The detection of sensor nonlinearities is shown to be equivalent to solving the largest empty rectangle (LER) problem, given a set of features extracted from an analysis of sensor outputs. A low-complexity algorithm that gives an approximate solution to the LER problem is proposed for embedment in resource constrained wireless sensors. By solving the LER problem, sensors corrupted by non-linearity faults can be isolated and identified. Extensive analysis evaluates the performance of the proposed algorithm through simulation.

1. Introduction

Wireless sensor networks (WSNs) have been widely adopted in many engineering domains and applications including in structural monitoring [1], environmental monitoring [2], battlefield surveillance [3] and animal tracking [4]. Interest in WSNs is directly attributed to the benefits of not having to install wires in a system and to the mobility offered when untethered. For reliable system monitoring and subsequent data-based decision making, it is necessary to have accurate sensor measurements. However, in order to reduce the cost and size of wireless sensors, commercial off-the-shelf components are typically used in their design; these components can be vulnerable in harsh field settings. Given the fact that WSNs are usually deployed in demanding operational environments, wireless sensors are potentially more prone to failure than wired counterparts. Hence, automated sensor diagnosis algorithms that allow wireless sensors to self-diagnose errors in their measurements are direly needed.

A great deal of research has been conducted over the past decade to develop sensor diagnosis methods with many of them designed explicitly for WSNs. Sensor malfunctions can be classified into two broad categories: sensor failure and sensor faults. Sensor failure refers to a sensor's inability to report its data or to respond to user commands. The causes of sensor failure can be the breakdown of the hardware components or simply from the depletion of available power in the

* Corresponding author at: Department of Civil and Environmental Engineering, University of Michigan, Ann Arbor, MI 48109-2125, USA. Tel.: +1 734 615 5290.
E-mail addresses: chunlo@umich.edu (C. Lo), jerlynch@umich.edu (J.P. Lynch), mingyan@umich.edu (M. Liu).

http://dx.doi.org/10.1016/j.ymssp.2015.05.011
0888-3270/

case of battery-operated sensors. The method of detecting failed sensors is to send a query to the sensor and to check whether the sensor responds. Highly efficient and accurate failed sensor detection algorithms have been published in recent years [5–7]. The second type of sensor malfunction is sensor fault, which refers to a situation where a sensor is able to report its observations but the reported data is corrupted. Sensor faults are significantly more difficult to detect than failure because investigation of the correctness of the reported observations (*i.e.*, measurements) is required. The process of sensor fault diagnosis can be classified into four steps: (1) detection (detecting whether there are any faulty sensors in the system), (2) isolation (determining which sensor(s) is(are) faulty), (3) identification (determining the type of faults that occurred) and (4) recovery (estimating the correct output of the faulty sensors). Most of the published studies only focus on the detection and isolation steps; comparatively, few have emphasized fault identification and recovery. The main approach being used for detecting sensor faults is to utilize analytical redundancies that exist in the system [8]. This general strategy assumes that sensors deployed to the same physical system should be correlated to some extent. This correlation can therefore be exploited for the diagnosis of sensor faults.

The sensor fault detection schemes proposed in the literature can be further classified into two more categories: model-based and model-less methods. Model-based sensor fault detection methods rely on knowledge of the underlying system in the form of a model that offers analytical redundancies [9–13]. The system model can be acquired by the physical properties of the system (*i.e.*, physics-based) or learned from the historical data of the system (*i.e.*, data-driven). Data-driven methods are specially valuable when the system being monitored is too complex to be modeled analytically. The acquired system model then acts as a fundamental reference system for sensor fault diagnosis. For example, Da and Lin [9] and Kobayashi and Simon [10] both proposed a centralized sensor fault diagnosis method that uses a bank of Kalman filters to represent the system. Both methods assume that the system is linear with the system model formulated in a state-space form. For a network of N sensors, an N-Kalman filter system is established such that the ith Kalman filter is based on all but the ith sensor. Assuming that there is only one faulty sensor in the network, exactly one Kalman filter (out of the N Kalman filters) behaves differently from the others. Therefore, the faulty sensor can be detected and isolated. The difference between these methods is that Da and Lin's method measures the discrepancies on the sensor observations while Kobayashi's method measures the discrepancies on the state vector of the state-space model. In Xu et al. [12], a sensor fault diagnosis method based on artificial neural network (NN) models is proposed. A NN model is used to capture the correlations between a group of sensors based on the sensors' historical data. When one sensor (or a small number of sensors) becomes faulty, its output will be inconsistent with predictions of that sensor's output based on the other sensors' outputs. Dunia et al. [13] and Kerschen et al. [14] proposed a fault detection method based on Principal Component Analysis (PCA) models. Their studies assumed that the sensors are highly correlated and that their outputs can be captured in a more compact dimensional space (which is regarded as the principal components) than the original observation space. When the dynamics of a sensor's observations are not concentrated on the principal components, the sensor is regarded as potentially faulty. Dunia et al. [13] further analyzed how different types of faults affect the PCA residuals, thereby providing a tool to identify the fault types occurring in the faulty sensors. All of these model-based methods are centralized methods where a base-station has knowledge of the system model, collects observations from the sensors, and performs the fault diagnosis.

A challenge of model-based methods for fault detection in WSNs is that communication of data in the network consumes a large amount of energy. Due to the limited energy available at each wireless sensor, reduction of communication between sensor nodes is preferred. As a result, numerous studies have explored distributed fault diagnosis methods that generally require less data transmissions [15–18]. These methods tend to be model-less methods where a simple assumption is made: sensors in close proximity will observe similar signals. Because of this assumption, the diagnosis algorithm is usually easily formulated in a distributed fashion. For instance, Ding et al. [17] assumed that sensors in close proximity should have similar outputs. Therefore, their method has each sensor comparing its output with the mean output value of its neighboring sensors. If the sensor output is much bigger than that of its neighboring sensors, the sensor is regarded as faulty. Another model-less distributed method was proposed by Luo et al. [18] for event-detection WSNs. In this study, each sensor reports the occurrence of an event. Assuming sensor faults are stochastically unrelated, a final decision of the event state is made by a majority vote from the individual decisions of a group of sensors. Sensors that frequently give different results are considered to be faulty. The study also determined the optimal number of sensors in a group and the optimal threshold for majority voting based on the probability for a sensor to be faulty. Although these model-less diagnosis methods are distributive and have lower energy requirements, they also often impose limitations based on the assumptions made in their derivations.

In this study, a model-based distributed sensor fault detection method is proposed. The proposed method fills the gap between model-based centralized methods and model-less distributed methods. To fill this gap, the strategy presented will be tailored to search for a specific fault type. This allows the fault diagnosis algorithm to be capable of performing the first three steps: detection, isolation and identification. The proposed fault diagnosis algorithm specifically focuses on identifying non-linearity faults that exist in the sensor's transfer function. Non-linearity faults are a multiplicative error which means that the error is a function of the true signal. In this study, a sensor that suffers from a non-linearity fault (*i.e.*, a nonlinear transfer function) has normal and abnormal operating regions. A sensor gives correct measurement when the true signal is within the normal region and gives distorted measurement when the true signal falls in the abnormal region. This is a common characteristic in many sensors. For instance, some sensors (*e.g.*, amplifiers) suffer from nonlinear distortions when the input signal is close to their operating limits. Piezoelectric sensors also observe a large (undesired) gain in their transfer function when the input signal gets close to the sensors' resonant frequencies [19]. Nonlinearities can also be introduced

Please cite this article as: C. Lo, et al., Distributed model-based nonlinear sensor fault diagnosis in wireless sensor networks, Mech. Syst. Signal Process. (2015), http://dx.doi.org/10.1016/j.ymssp.2015.05.011

when a sensor is not properly mounted to the system being observed. For example, high amplitude responses can induce relative motion between a sensor and a structure if the sensor is not properly bonded to the surface of the structure. Operating in an abnormal region of a sensor is usually prevented by examining the characteristics of the sensor and ensuring it remains in its normal operating region. However, the characteristics of a sensor could change with time or by unexpected events leading to operation in the abnormal region. For example, piezoelectric sensors could experience degradation over time in the bond between the sensor and the structure [20]. Amplifier-based sensors suffer from narrower linear operating ranges when their supply voltages drop. Moreover, the characteristics of a sensor can be significantly affected by operating environment (*e.g.*, temperature) and component aging [21]. Therefore, keeping the operation of a sensor in the normal range cannot guarantee the elimination of non-linearity faults in sensors.

A methodology which is able to detect and identify non-linearity faults is essential to ensuring the quality and functionality of WSNs. In this paper, preliminaries of the proposed decentralized sensor fault detection method and the characteristics of non-linearity faults are presented in Section 2. The methodology of the fault detection and identification algorithm is presented in Section 3. Section 4 quantitatively evaluates the algorithm performance through simulation studies. Finally, Section 5 presents the study's conclusions and discusses future research directions.

2. Sensor observations and non-linear fault models

Previous work [22] showed that if the system being monitored is linear, a direct linear relationship exists between the output of any pair of sensors. Consider a linear system that is represented by a state-space model in the Z-domain:

$$z\mathbf{X}(z) = \mathbf{A}\mathbf{X}(z) + \mathbf{B}\mathbf{U}(z) \tag{1}$$

$$\mathbf{Y}(z) = \mathbf{C}\mathbf{X}(z) + \mathbf{D}\mathbf{U}(z) \tag{2}$$

where $\mathbf{X}(z) \in \mathbb{R}^n$ is the state vector of the system, $\mathbf{U}(z) \in \mathbb{R}^l$ is the input vector, and $\mathbf{Y}(z) \in \mathbb{R}^m$ is the output vector of the sensors. Furthermore, $\mathbf{A} \in \mathbb{R}^{nxn}$ is the state transition matrix which defines the transition of system states, $\mathbf{B} \in \mathbb{R}^{nxl}$ is the input matrix which represents the relationship between the input and the system state, $\mathbf{C} \in \mathbb{R}^{mxn}$ is the output matrix, and $\mathbf{D} \in \mathbb{R}^{mxl}$ is the feed-through matrix.

By eliminating $\mathbf{X}(z)$ in (2) using (1), the transfer function $H_{pq}(z)$ between the outputs of sensors p and q, $Y_p(z)$ and $Y_q(z)$ respectively, can be represented by

$$H_{pq}(z) = \frac{Y_p(z)}{Y_q(z)} = \frac{(\mathbf{C}_p(z\mathbf{I}-\mathbf{A})^{-1}\mathbf{B} + \mathbf{D}_p)\mathbf{U}(z)}{(\mathbf{C}_q(z\mathbf{I}-\mathbf{A})^{-1}\mathbf{B} + \mathbf{D}_q)\mathbf{U}(z)} \tag{3}$$

where the subscript p (or q) on $\mathbf{C}$ and $\mathbf{D}$ represent the pth (or qth) rows of these matrices. Eq. (3) can be equivalently written as

$$H_{pq}(z) = \frac{\sum_{j=0}^{n}(\sum_{i=1}^{l} U_i\alpha_{ij})z^j)}{\sum_{j=0}^{n}(\sum_{i=1}^{l} U_i\beta_{ij})z^j)} \tag{4}$$

where the coefficients α_{ij} and β_{ij} ($i = 1, \ldots, l$ and $j = 1, \ldots, n$), are determined by the state-space model matrices (*i.e.*, $\mathbf{A}, \mathbf{B}, \mathbf{C}$ and $\mathbf{D}$). Therefore, the relationship between any two sensors depends on their historical observations and the excitation inputs to the system. If the excitation inputs can be aggregated as a single source (*i.e.*, $l = 1$), the relationship is independent of the system input:

$$\frac{Y_p(z)}{Y_q(z)} = \frac{\alpha_n z^n + \alpha_{n-1} z^{n-1} + \cdots + \alpha_1 z + \alpha_0}{\beta_n z^n + \beta_{n-1} z^{n-1} + \cdots + \beta_1 z + \beta_0} \tag{5}$$

Modeling system inputs as a single source is quite common in many engineering systems. For example, building structures exposed to ground motions (*e.g.*, earthquakes) and mechanical systems excited by ambient Gaussian inputs reduce to a single input system. In order to simplify the discussion, a single-input system is assumed in the rest of the study. However, the discussion remains valid for multiple-input systems if the inputs are known or measurable.

When a system is too complex (or it is too expensive) to acquire the complete state space model parameters, the relationship (transfer function) between a pair of sensors, y_p and y_q, can be captured by a time series model (such as an autoregressive with exogenous input (ARX) time-series model [23]) trained from historical sensor outputs:

$$\sum_{i=0}^{\nu_1} \alpha_i y_q(k-i) = \sum_{i=0}^{\nu_2} \beta_i y_p(k-i). \tag{6}$$

where ν_1 and ν_2 are the orders of the model.

An ARX model is a low complexity model that can be easily implemented in wireless sensors as has been done in the past [24]. Fast iterative ARX model fitting algorithms are also available [25]. The execution of these methods is based on the Yule–Walker equations, which is a bi-Toeplitz system (a matrix consisting of 2×2 block Toeplitz matrices) for the ARX model. Based on the structure of the bi-Toeplitz system of successive system orders, the model parameters of a system can be

Please cite this article as: C. Lo, et al., Distributed model-based nonlinear sensor fault diagnosis in wireless sensor networks, Mech. Syst. Signal Process. (2015), http://dx.doi.org/10.1016/j.ymssp.2015.05.011

calculated from the parameters of the next lower-order system. This method requires $O((m+n)^2)$ calculations and $O(m+n)$ storage on the wireless sensor.

Non-linearity faults are multiplicative measurement errors which depend on the sensor output. A non-linearity fault can be represented by a nonlinear transfer function between the true signal and the output of the sensor. The function (Fig. 1) has two regions: normal and abnormal. When the actual signal is within the normal region, the measurement correctly reflects the actual signal. When the sensor signal falls into the abnormal region, the sensor transfer function is altered leading to errors in the measurement. In this study, two simplified non-linearity models are used. The first one is the bilinear model of Fig. 1. Within the normal region, the measurement is exactly equal to the true signal. Within the abnormal region(s), which is the compliment of the normal region, the function between the measurement and true signal follows another linear function with a different slope. The mathematical expression of the bilinear model is

$$y=\begin{cases} x & \text{if } r_2<x<r_1,\\ \tan(\theta_1)(x-r_1)+r_1 & \text{if } x\geq r_1,\\ \tan(\theta_2)(x-r_2)+r_2 & \text{if } x\leq r_2. \end{cases} \tag{7}$$

where x is the actual signal, y is the sensor measurement and $r_1>0, r_2<0$ define the boundaries of the normal region. Moreover, the slopes θ_1 and θ_2 have the range $[0,\pi/2)$. The parameters of the bilinear model are the normal region boundaries, r_1 and r_2, and the slope of the linear profile in the abnormal region, θ. A non-linear model can have either one-sided or two-sided abnormal region(s). For example, if $r_1<\infty$ and $r_2=-\infty$, we have a one-sided abnormal region. The measurement-true signal transfer function of (7), as illustrated in Fig. 1, is used to model the measurement of a sinusoidal signal with unit amplitude. The bilinear fault is assumed to be one-sided with $r_1=0.6$ and $r_2=-\infty$; also, $\theta_1=30^\circ$. As shown in Fig. 2, the faulty signal is evident in the positive amplitude with the amplitude lower than the true signal amplitude.

The second non-linear model uses exponential functions to model the sensor's abnormal region(s). Within the normal region, the measurement is equal to the actual signal. Within the abnormal region, the function between the measurement and true signal follows an exponential profile as defined by

$$y=\begin{cases} r_2 & \text{if } r_2<r_1,\\ \max\{r_2-(\exp(\psi|r_2-r_1|)-1), \frac{1}{\psi}\ln\frac{1}{\psi}-\frac{1}{\psi}+r_1+1\} & \text{if } r_2\geq r_1,\ \texttt{Type I}\\ \max\{r_2+(\exp(\psi|r_2-r_2|)-1), -\frac{1}{\psi}\ln\frac{1}{\psi}+\frac{1}{\psi}+r_2-1\} & \text{if } r_2\leq r_2,\ \texttt{Type I}\\ r_2+(\exp(\psi|r_2-r_1|)-1) & \text{if } r_2\geq r_1,\ \texttt{Type II}\\ r_2-(\exp(\psi|r_2-r_1|)-1) & \text{if } r_2\leq r_2,\ \texttt{Type II}. \end{cases} \tag{8}$$

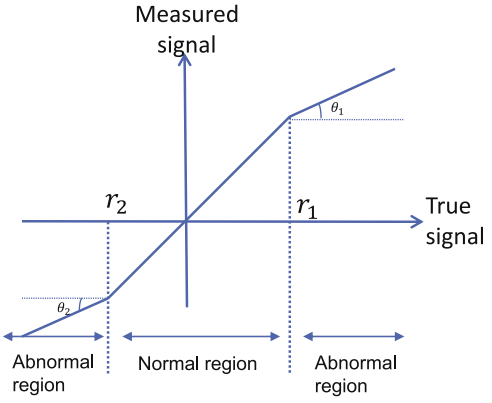

Fig. 1. Bilinear non-linear sensor fault model.

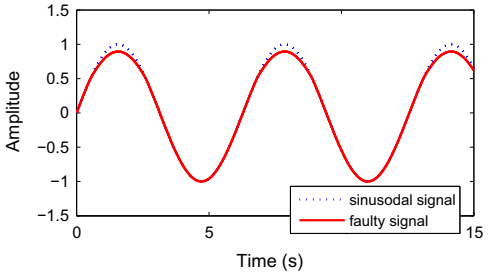

Fig. 2. A unit amplitude sinusoidal signal and the corresponding non-linearity faulty measured signal with $r_1=0.6$, $r_2=-\infty$ and $\theta_1=30^\circ$.

Please cite this article as: C. Lo, et al., Distributed model-based nonlinear sensor fault diagnosis in wireless sensor networks, Mech. Syst. Signal Process. (2015), http://dx.doi.org/10.1016/j.ymssp.2015.05.011

where ψ, r_1 and r_2 (with $r_1 > 0$ and $r_2 < 0$) are the parameters of the model. Compared to the bilinear model, the function of the exponential model has a gradual change from the normal region to the abnormal region. Fig. 3 shows the functions of a one-sided exponential with varying model parameter ψ and with normal region boundary set at $r_1 = 30$. The output saturation problems of amplifier-based sensors, where measurements are smaller than the actual signal, are best modeled by the exponential nonlinear fault model (Type I). On the other hand, excessive gain problems (such as sensor resonance), where measurements are larger than the actual signal are best model by Type II exponential functions.

3. Non-linearity fault detection and identification methodology

Consider a N-sensor WSN where each sensor has the potential to suffer from non-linearity faults but the network has no knowledge of which sensors are normal. The WSN is partitioned into peer-to-peer sensor pairs as shown in Fig. 4 (*e.g.*, $y_2 - y_4, y_1 - y_3, y_5 - y_6$ and $y_6 - y_7$). As mentioned in the previous section, the relationship between any pair of sensors can be captured by an ARX model trained using sensor outputs and (6). The model parameters can be learned from the historical data by a fast iterative algorithm [25] when the sensors are working normally. Fig. 5 provides an overview of the detection method proposed to detect and identify non-linearity faults within a pair of sensors. There is no *a priori* knowledge of the health of sensor 1 or 2 in this approach (*i.e.*, both could be faulty). The first sensor, S_1, transmits it output, $\tilde{y}_1$, to the second sensor, S_2. S_2 then uses its measured output, $\tilde{y}_2$, to predict S_1's output, $\hat{y}_1$, using a previously trained ARX model between the $S_1 - S_2$ pair. The difference between the estimated signal, $\hat{y}_1$, and measured signal, $\tilde{y}_1$, constitutes a cross-error function, which represents the signal measurement accuracy of the sensor pair. As will be described, this error function will be analyzed to extract feature points (say P_{S_1} and P_{S_2}) which are useful for fault detection and identification. Under the largest empty rectangle (LER) identification process, the faulty sensor(s) within the sensor pair can be isolated and the non-linear

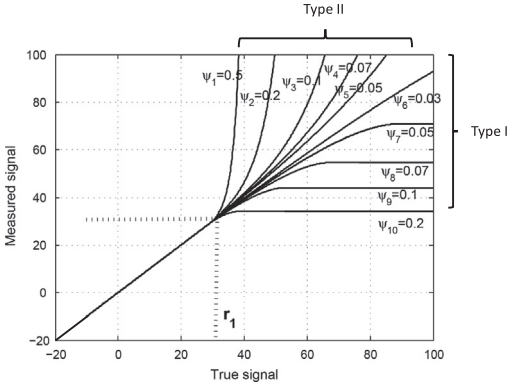

Fig. 3. Exponential non-linearity sensor fault model (one-sided version shown).

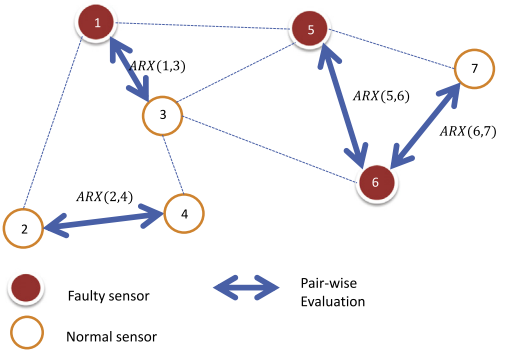

Fig. 4. Pair-wise fault detection in a sensor network.

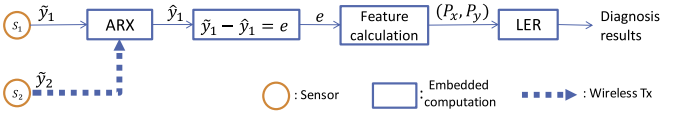

Fig. 5. Overview of detecting and identifying non-linearity faults within the $S_1 - S_2$ pair.

Please cite this article as: C. Lo, et al., Distributed model-based nonlinear sensor fault diagnosis in wireless sensor networks, Mech. Syst. Signal Process. (2015), http://dx.doi.org/10.1016/j.ymssp.2015.05.011

fault model parameters can be identified. This fault diagnosis process can be carried out in parallel between each sensor pair and thus the proposed fault diagnosis method is scalable as the size of a WSN grows. In the rest of this section, each component of the fault diagnosis methodology will be discussed in detail.

3.1. Cross-error function

Using the stored ARX model with ν coefficients, the prediction of S_1's output, $\hat{y}_1(k)$, at time k can be calculated by the measured outputs of $\tilde{y}_1$ and $\tilde{y}_2$:

$$\hat{y}_1(k) = \sum_{i=1}^{\nu} -a_i\tilde{y}_1(k-i) + \sum_{i=0}^{\nu} b_i\tilde{y}_2(k-i). \tag{9}$$

where $a_i = \alpha_i/\alpha_0$ and $b_j = \beta_j/\alpha_0$ for $i = 1, \ldots, \nu$, and $j = 0, \ldots, \nu$.

As previously mentioned, S_1 and/or S_2 may be faulty. Let $e_1(k)$ be the observation error of S_1 at time k, then the observation of S_1, $\tilde{y}_1(k)$, is equal to $y_1(k)+e_1(k)$. Define the cross-error function, $e_{12}(k)$, to be the difference between the observed output and estimated output, we have

$$e_{12}(k) = \tilde{y}_1(k) - \hat{y}_1(k) \tag{10}$$

$$e_{12}(k) = \sum_{i=0}^{\nu} a_i e_1(k-i) - \sum_{i=0}^{\nu} b_i e_2(k-i) \tag{11}$$

The cross-error function represents the discrepancy between a pair of sensors. As a result, general faults can be detected by monitoring whether the cross-error function exceeds a threshold. It should be noted that the cross-error function reduces error information from the two sensors into a scalar value. As a result, it is difficult to identify which sensor is faulty and what type of fault it belongs to when there is a lack of additional information (*e.g.*, definition of a fault-free reference sensor). In the following subsection, a method that is able to isolate the faulty sensor and that identifies the non-linearity fault is presented.

3.2. Feature point calculation

Before introducing the non-linearity identification method, the sensor output is assumed to transgress into the abnormal region of the non-linearity fault model occasionally. In other words, the normal region of the sensor covers a significant portion of the signal range. This assumption is valid for most systems if appropriate sensors (with large enough dynamic range) are chosen for the monitoring task. In (11), the cross-error function utilizes past outputs of S_1 and S_2 over a time window from time 0 to time $-\nu$ (relative to the discrete-time index, k, of the cross-error function in (11)). The cross-error function is non-zero whenever a measurement error (*i.e.*, where the abnormal range is entered) occurs within the ARX lag window on any sensor. It should be noted that it is possible that errors between two sensors can cancel each other out, but this is an extremely rare event. Therefore, when the cross-error function is zero, it is almost certain that there is no fault within the time window. However, when the cross-error function is non-zero, it is uncertain when and which sensor the error occurred in unless it is the first time the cross-error function output deviates from zero (or near zero). This is because the cross-error function output can only be non-zero due to an error initiating at time k in one or both of the sensors. The measurement value of the faulty sensor at the time the cross-error function experiences its first non-zero value should fall in the abnormal region and thus have magnitude bigger than r_1 or r_2 if the sensor is corrupted by a non-linearity fault. However, it is not clear which sensor(s) is (are) faulty as the normal region boundaries (r_1, r_2) of the non-linearity model remain unknown. As such, a feature point, $\mathbf{P}$, is defined as $\mathbf{P} = (P_{S_1}, P_{S_2})$, where P_{S_1} and P_{S_2} are the measurement values of both sensors ($\tilde{y}_1$ and $\tilde{y}_2$) at the time the cross-error function first deviates from zero and exceeds a pre-defined threshold. Therefore, the total number of feature points available is equal to the number of times the cross-error function exceeds the threshold. Fig. 6 shows an example of how the feature points are extracted. In this example, S_1 is faulty with a non-linearity fault and S_2 is normal. Fig. 6(a) and(b) are the true signals of sensors 1 and 2 (denoted as S_1 and S_2), respectively. Fig. 6(c) is the (corrupted) signal measured by faulty sensor 1, $\tilde{y}_1$, and Fig. 6(d) is the calculated cross-error function. As can be seen, four feature points are available in this example.

After a set of feature points, $\wp$, are generated over a time history, they can be plotted on a 2-dimension plane with the x-axis corresponding to S_1 (P_{S_1}) and the y-axis corresponding to S_2 (P_{S_2}). The plot will have the patterns shown in Fig. 7 when the errors are caused by a non-linearity fault. In Fig. 7, the dotted lines represent the boundaries of the normal region of a non-linearity model (if the sensor is faulty). When S_1 is corrupted by a non-linearity fault and S_2 is normal, the x-coordinates of the set of collected feature points fall in the abnormal region while the y-coordinates of the feature points can have any value. Therefore, the feature points only fall into the region highlighted in Fig. 7(a). Similarly, Fig. 7(b) shows the region where the feature points should fall when S_1 is normal and S_2 is corrupted by a non-linearity fault. When both sensors are corrupted by a non-linearity fault, the collected data should fall in the highlighted regions in Fig. 7(c).

Consequently, if the sensor pair under investigation can be classified into one of the 3 different patterns in Fig. 7, the faulty sensor(s) can be isolated even if there are no reference sensors. Furthermore, as corrupted measurements should have

Please cite this article as: C. Lo, et al., Distributed model-based nonlinear sensor fault diagnosis in wireless sensor networks, Mech. Syst. Signal Process. (2015), http://dx.doi.org/10.1016/j.ymssp.2015.05.011

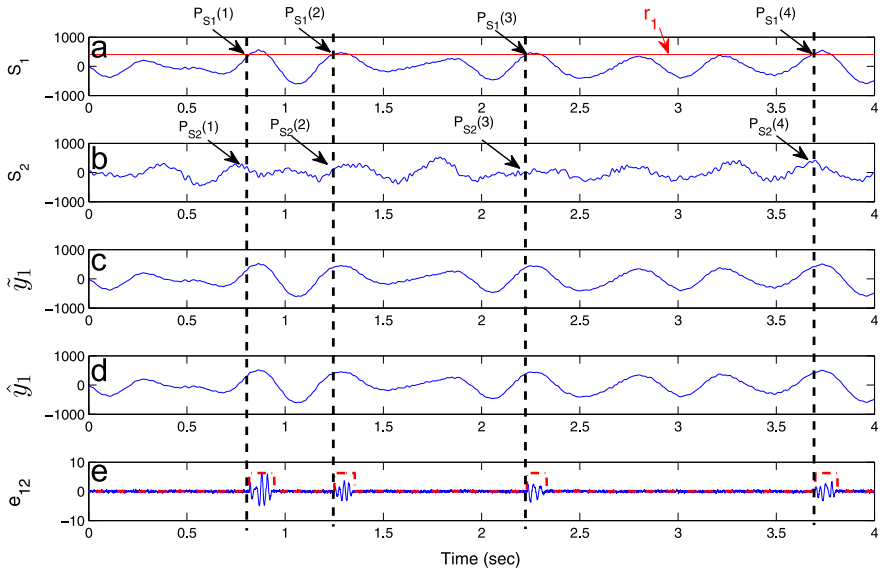

Fig. 6. Abnormal signal detection and feature point extraction: (a) true signal of S_1 (y_1), (b) true signal of S_2 (y_2), (c) measured signal from S_1 ($\tilde{y}_1$), (d) the predicted S_1 output ($\hat{y}_1$), and the (e) cross-error function (e_{12}) of the sensor pair.

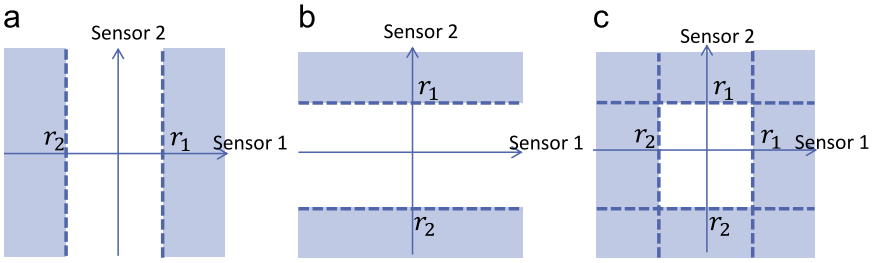

Fig. 7. Location (shaded area) of extracted feature points when: (a) S_1 is faulty and S_2 is normal, (b) S_1 is normal and S_2 is faulty and (c) both S_1 and S_2 are faulty. The dotted lines correspond to the boundaries between the normal and abnormal regions.

values outside the normal region, the normal region boundaries can also be detected from the collected data. In fact, this classification problem can be modeled as the largest empty rectangle problem (LER) with a query point [26,27]. Given a set of points and the boundaries in a 2-D space, the largest empty rectangle problem is to find the largest rectangle (with sides parallel to the axes) that does not contain any of the given points but contains the query point. Moreover, this rectangle should locate within the boundaries which can be set to be slightly larger than the maximum amplitudes of the given points. The non-linearity fault isolation and identification problem is equivalent to identifying the largest empty rectangle that contains the origin. The sides of the largest empty rectangle which intercept with the x-axis (y-axis) illustrate the parameters (*i.e.*, r_1 and r_2) of the non-linearity fault in sensor 1 (sensor 2). When a side is collocated with the boundary, it means no fault is detected on that region given the collected data; otherwise the coordinate of the side represents the range of the normal region of the non-linearity model.

3.3. *Largest empty rectangle (LER) problem*

Finding the largest empty rectangle is an important problem in many applications including VLSI layout optimization [28] and database management [27]. Given its ubiquitous nature, many algorithms have been developed to solve this problem. However, even one of the faster algorithm [26] requires $O(N\phi(N)\log^4(N))$ operations, where N is the number of given points and $\phi(N)$ is the slowly increasing inverse Ackermann function [29]. This requirement is quite demanding for low power wireless sensors when the size of the collected data is large. Therefore, a more efficient algorithm that finds an approximate largest empty rectangle containing the origin is proposed. The main concept of the algorithm is to first find a small rectangle that does not contain any given points and then to enlarge the rectangle by expanding the sides separately. The proposed method, which requires $O(N)$ operations, is shown in Algorithm 1. In the algorithm, $\wp$ is the set of collected feature points ($x_{max}, x_{min}, y_{max}$ and y_{min}) define the boundaries and v_x (v_y) represents the x-coordinate (y-coordinate) of a point v.

Please cite this article as: C. Lo, et al., Distributed model-based nonlinear sensor fault diagnosis in wireless sensor networks, Mech. Syst. Signal Process. (2015), http://dx.doi.org/10.1016/j.ymssp.2015.05.011

Algorithm 1. Approximate largest empty rectangle algorithm.

Require $\wp, x_{max}, x_{min}, y_{max}, y_{min}$

Calculate the shortest distance d of the points in the set $\wp$ from the origin: $d = \min\{\sqrt{P_{S_1}^2 + P_{S_2}^2} | \mathbf{P} \in \wp\}$

Construct an empty rectangle with sides: $x_{pos} = d, x_{neg} = -d, y_{pos} = d, y_{neg} = -d$

Subroutine 1:

$Q = \{v \in \wp | y_{pos} \geq v_y \geq y_{neg}\}$

$x_{pos}^1 = \min\{x_{max}, \{v_x \in Q | v_x \geq 0\}\}$

$x_{neg}^1 = \max\{x_{min}, \{v_x \in Q | v_x < 0\}\}$

$Q = \{v \in \wp | x_{pos}^1 \geq v_x \geq x_{neg}^1\}$

$y_{pos}^1 = \min\{y_{max}, \{v_y \in Q | v_y \geq 0\}\}$

$y_{neg}^1 = \max\{y_{min}, \{v_y \in Q | v_y < 0\}\}$

$A_1 = (x_{pos}^1 - x_{neg}^1) \times (y_{pos}^1 - y_{neg}^1)$

Subroutine 2:

$Q = \{v \in \wp | x_{pos} \geq v_x \geq x_{neg}\}$

$y_{pos}^2 = \min\{y_{max}, \{v_y \in Q | v_y \geq 0\}\}$

$y_{neg}^2 = \max\{y_{min}, \{v_y \in Q | v_y < 0\}\}$

$Q = \{v \in \wp | y_{pos}^2 \geq v_y \geq y_{neg}^2\}$

$x_{pos}^2 = \min\{x_{max}, \{v_x \in Q | v_x \geq 0\}\}$

$x_{neg}^2 = \max\{x_{min}, \{v_x \in Q | v_x < 0\}\}$

$A_2 = (x_{pos}^2 - x_{neg}^2) \times (y_{pos}^2 - y_{neg}^2)$

if $A_1 \geq A_2$

then

Output LER with sides: $\{x_{pos}^1, x_{neg}^1, y_{pos}^1, y_{neg}^1\}$

else

Output LER with sides: $\{x_{pos}^2, x_{neg}^2, y_{pos}^2, y_{neg}^2\}$

end

As can be easily verified, the rectangles calculated from subroutines 1 and 2 do not contain any feature points but do contain the origin. Each side of the rectangle either touches at least one data point or is collocated with one of the boundaries (x_{max} and/or y_{max}). The difference between subroutines 1 and 2 is the direction (x- or y-directions) the rectangle expands first. The bigger rectangle is used for fault isolation and identification.

The assumption declared at the outset assumes that the normal region of the faulty sensors covers a significant dynamic range of the signal. As a result, the area of the discovered largest empty rectangle should be comparable to the product of the maximum signal amplitudes of the two sensors (due to large r_1 and r_2). If the corruption of measurement is not due to a non-linearity fault, errors can occur at any signal amplitude and the largest empty rectangle found by the proposed algorithm would have a small area if the number of collected data points is large enough. An illustration of this property can be found in Section 4.3.

Fig. 8 shows an example of how the proposed largest empty rectangle algorithm identifies non-linearity faults. The data shown in the figure is extracted from a simulation experiment; the details of the experiment can be found in Section 4. In Fig. 8, the circular markers represent the set of feature points, P. The solid lines of the outer rectangle represent the boundaries of the largest empty rectangle problem. The dotted rectangle represents the final identified LER by Algorithm 1. As the top and bottom sides of the rectangle are collocated with the outer rectangle boundaries, there is no fault on S_2. However, S_1 is corrupted by non-linearity faults and the normal region of the fault is defined by the x-coordinates of the left and right sides of the rectangle.

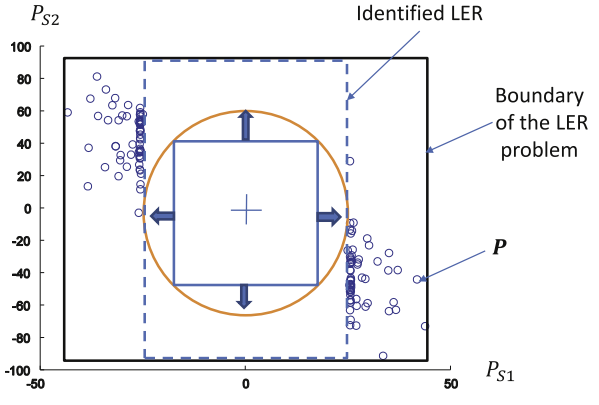

Fig. 8. Illustration of the sub-optimal LER detection algorithm proposed to identify non-linear fault types in the two sensors.

Please cite this article as: C. Lo, et al., Distributed model-based nonlinear sensor fault diagnosis in wireless sensor networks, Mech. Syst. Signal Process. (2015), http://dx.doi.org/10.1016/j.ymssp.2015.05.011

4. Simulation and results

In this section, the performance of the proposed algorithm is investigated including validation of its ability to detect and isolate sensors with non-linearity faults. The detection performance will be evaluated over different system excitations and under different non-linearity models. The diagnosis algorithm performance using the optimal LER and the proposed sub-optimal LER algorithms will be investigated. Also, the relationship between the detection accuracy and the number of collected feature points will be explored.

4.1. System for validation

A 5-degree-of-freedom lumped mass dynamical system (Fig. 9) is adopted for simulation experiments. A lumped mass dynamical system is able to model different type of physical systems, such as bridges, vehicles, machines, among others [30,22]. The masses, m_i, are connected via discrete springs and viscous dampers with spring constants, k_i, and damping coefficients, c_i, respectively. An external force, $u_i(k)$, is applied to each mass. Each mass also has a translational degree-of-freedom, x_i. In this study, similar model parameters used in [30] are adopted: each mass is set to 1 kg with each spring constant and damping coefficient set to 10 kN/m and 10.5 Ns/m, respectively. Under these model parameters, the system has natural frequencies at 4.52, 13.22, 20.84, 26.78, and 30.54 Hz. Each mode of vibration is under-damped with damping ratios of 1.5%, 4.4%, 6.8%, 8.8%, and 10.1% for mode 1 (4.52 Hz) through 5 (30.54 Hz), respectively. The vibration of the system is recorded as the acceleration of each degree-of-freedom ($y_i = \ddot{x}_i$) with a sampling rate of 200 Hz. The excitation inputs on each degree-of-freedom are from a single source $u(k)$ but with different levels of magnification: $u_1 = 5u, u_2 = 1u, u_3 = 0.2u, u_4 = -1.5u, u_5 = 12.2u$.

4.2. Simulation methodology

In this experiment, two types of excitation are used. The first excitation is a double-tone harmonic signal. The two frequencies of the signal are randomly chosen between 2 and 8 *Hz* using a uniform distribution. In a similar fashion, the magnitude of each tone is also randomly and uniformly chosen between 10 and 13 N. The second excitation is a white noise signal. When fitting ARX models between sensor pairs, the order of the ARX model is set to $\nu = 20$.

For each simulation, whether a sensor is faulty or not is decided with equal probability ($p = 0.5$). Also, it is decided at the outset what non-linearity fault model will be used (bilinear versus exponential). However, whether the non-linearity is one-sided on the positive side, one-sided on the negative side, or both-sided is determined randomly with equal probability assigned to each case. The ARX coefficients are trained by sensor outputs when independent white noise excitations are applied. During performance evaluation, a pair of sensors is randomly chosen and then the proposed algorithm for fault diagnosis is applied. A threshold on the cross-error function is used to determine whether there are discrepancies between a pair of sensors. In the following experiments, the threshold is set to the maximum amplitude of the cross-error function output when both sensors are functioning normally (or during the training of the ARX model). The proposed sub-optimal LER algorithm is used for all the experiments except when evaluating the differences in performance between the optimal and sub-optimal LER algorithms. For all of the experiments, unless another noise value is explicitly stated, a zero-mean Gaussian white noise with variance of 0.5% of the maximum amplitude of the sensor measurements is superimposed to simulate measurement noise.

4.3. Simulation results

In the first experiment, the detection performance of the proposed algorithm is evaluated over different parameters of the bilinear and exponential non-linearity models. Three performance criteria are evaluated. The first criterion is the percentage of faulty sensors that are correctly detected to be faulty (*i.e.*, detection rate and denoted as "DR" in the legends of the figures). The second criterion is the percentage of normal sensors falsely detected as faulty (*i.e.*, false alarms and denoted as "FA" in the legends of the figures). The third criterion is, among the correctly detected faulty sensors, the accuracy of detecting the abnormal region(s) of the non-linearity model. As the abnormal region can be one-sided or two-sided, we evaluate each side separately. For example, if an abnormal region appears on the positive side and the algorithm detects it correctly, a correct detection is recorded. This accuracy measure is denoted as abnormal region detection rate (*i.e.*, "Abn. region DR" in the legends of the figures).

Fig. 10(a) shows the performance when a bilinear non-linearity model is used. The x-axis of the plot represents the degree θ of the slope in the abnormal region (note that a normal slope is 45°). As can be seen, the proposed algorithm

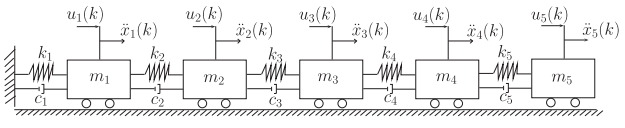

Fig. 9. Five degree-of-freedom (DOF) spring-mass-damper system for validation of the non-linearity fault diagnosis method.

Please cite this article as: C. Lo, et al., Distributed model-based nonlinear sensor fault diagnosis in wireless sensor networks, Mech. Syst. Signal Process. (2015), http://dx.doi.org/10.1016/j.ymssp.2015.05.011

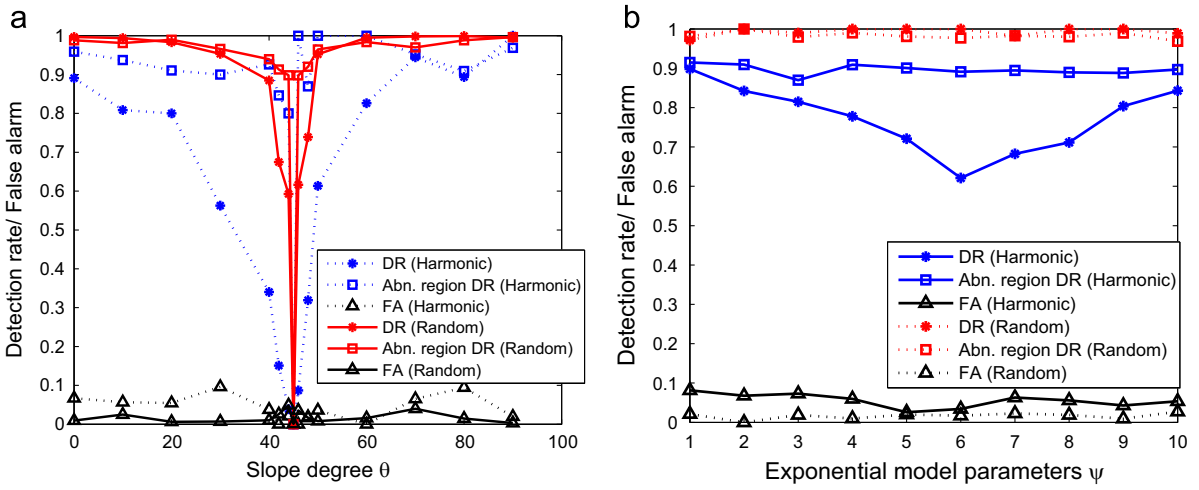

Fig. 10. Faulty sensor detection accuracy versus (a) different slope degree θ (bilinear model) and (b) variations in the exponential model parameter ψ.

achieved over a 90% detection rate and less than a 4% false alarm rate for most of the slope degrees when a white-noise excitation signal is used to excite the system. When a double-tone harmonic excitation is used, the detection rate is about 75% and the false alarm rate is about 7%. The difference in performance is because the sensor measurements of the white-noise excited system falls into the abnormal region rapidly and frequently. Consequently, the algorithm yields a more sensitive cross-error function and has better diagnosis accuracy. The detection rate decreases as the deviation is very close to the normal condition, (*i.e.*, 45°). This result is expected as the non-linearity error is also getting smaller and thus more difficult to detect from the cross-error function. The detection rate remains very high (at greater than 85%) when the slope deviates more than 10 ° from normal for white-noise excitations; this detection rate is greater than 65% for double-tone harmonic excitations. For detecting the abnormality type (*i.e.*, one-sided on the positive side, one-sided on the negative side, or two-sided) of the non-linearity model, the algorithm is able to achieve an accuracy of 90% for every deviation degree and for both system excitations. Note that for zero faulty sensor detection rate, the abnormal type detection rate is simply set to 0.

The same experiment is repeated using the exponential non-linearity model with the results shown in Fig. 10(b). Similar to the bilinear model, white-noise excitations achieve better results than double tone harmonic excitations. When exciting the system harmonically, detection rates of 95% or greater are found. However, the double tone harmonic has a detection rate between 60 and 90% depending on ψ. When white noise excited, the detection rate does not show a significant drop in performance when the non-linearity model function is close to the normal function (ψ_6). However, when excited by the harmonic signal, the detection rate increases as the exponential nonlinearity is more dominant. Note that the *x*-axis of Fig. 10(b) represents various exponential model parameters ψ but the distance between them is not related to the error magnitude.

Apart from detecting and isolating the faulty sensors, another important capability of the proposed method is its ability to detect the boundary values of the normal region. Fig. 11 shows the histogram of boundary estimation accuracy under the bilinear non-linearity model with parameter $\theta = 30^\circ$ and white-noise excitation. Fig. 11(a) represents the white-noise excitation under the bilinear model, Fig. 11(b) represents harmonic excitation under the bilinear model, Fig. 11(c) represents the white-noise excitation under the exponential model and Fig. 11(d) represents the harmonic excitation under the exponential model. The estimation error is normalized (*i.e.*, the estimation error is divided by the actual boundary value). As can be seen, 95% of the estimations are within 2% of the actual boundary value for white-noise excitations and 80% of the estimations are within 3% of the actual boundary value for double-tone excitations. Most of the boundary estimations (except the harmonic excitation under the bilinear model case) are higher than the actual boundary value because the magnitude of the faulty measurements (thus the corresponding value of the selected feature points) is always larger than the true normal region boundary value. Therefore, the boundary values detected by the LER method are usually larger than the actual boundary values. This error can be reduced by using more feature points and avoiding unnecessarily large thresholds on the cross-error function. For the harmonic excitation under the bilinear model (Fig. 11(c)), more than half of the estimations are smaller than the actual boundary values. This is mainly because the feature points collected from the less sensitive cross-error function have lower accuracy. As can be seen from the results, the proposed algorithm is able to achieve high accuracy on the boundary value estimation, which is important in signal recovery or for preventing the sensor from being used in the abnormal region in the future.

The proposed sub-optimal LER method is used in all of the previous experiments. This method has much lower complexity than the optimal LER method but it does not guarantee the largest empty rectangle. Therefore, a comparison is performed to reveal differences in the accuracy of these two methods. The experiment is performed under the bilinear non-linearity model with white-noise excitations. The results (Fig. 12) show that the proposed low complexity LER method is

Please cite this article as: C. Lo, et al., Distributed model-based nonlinear sensor fault diagnosis in wireless sensor networks, Mech. Syst. Signal Process. (2015), http://dx.doi.org/10.1016/j.ymssp.2015.05.011

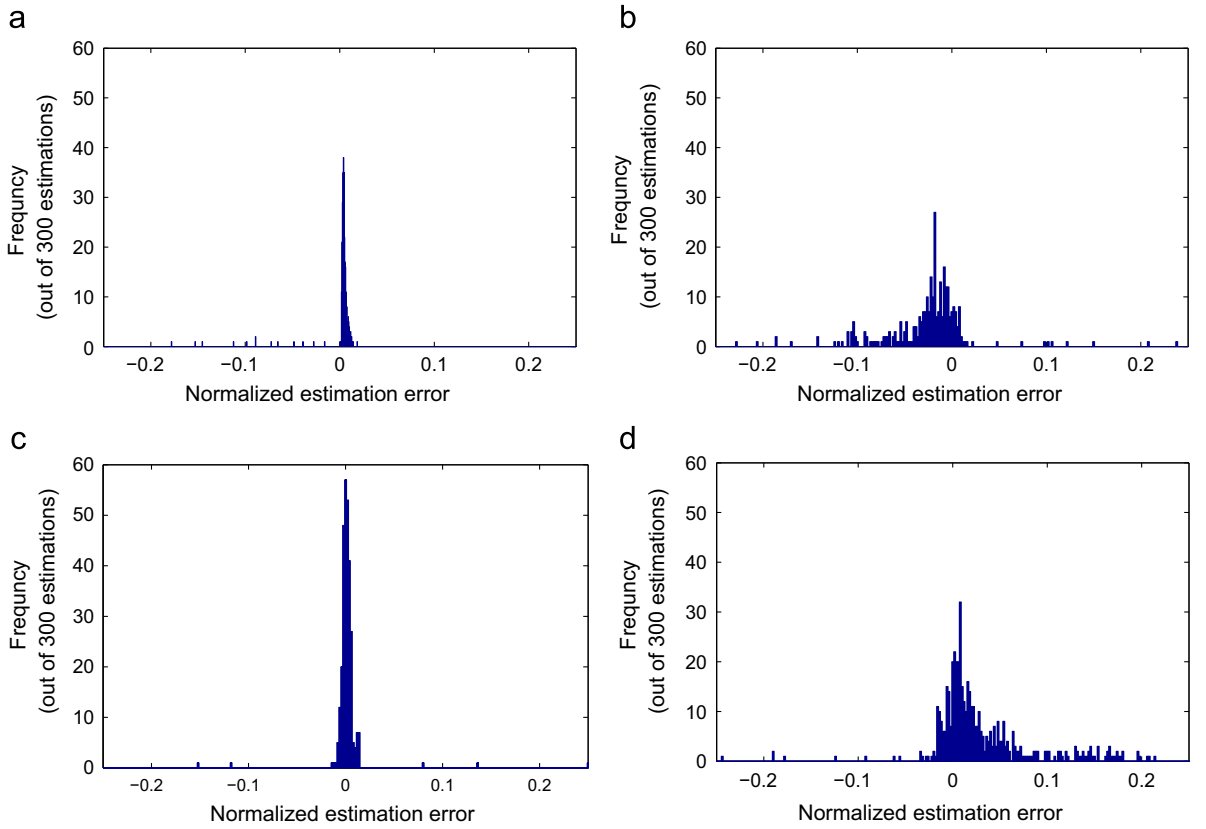

Fig. 11. Normalized normal region boundary detection accuracy: (a) White noise excitation under bilinear model, (b) harmonic excitation under bilinear model, (c) White noise excitation under exponential model and (d) harmonic excitation under exponential model.

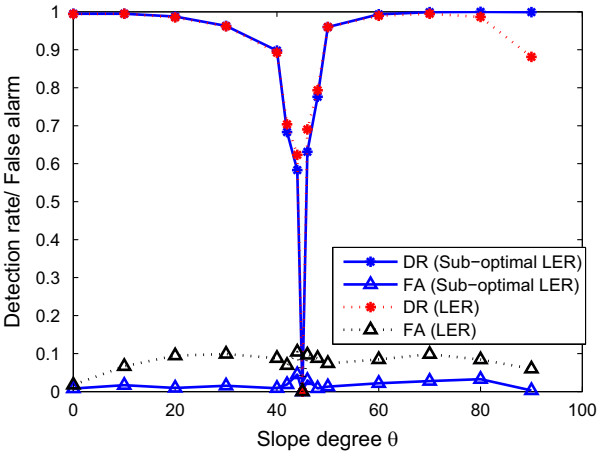

Fig. 12. Comparison of detection performance between using the optimal LER method and the proposed low complexity LER method.

able achieve similar detection rates as the optimal LER method. Although the optimal method achieves a higher level of accuracy when the non-linearity error is small (*i.e.*, when θ is close to 45°), the optimal method generally has a higher false alarm rate. Similar results are also observed for the exponential non-linearity model. Therefore, for detecting non-linearity faults, the proposed low complexity LER method is deemed sufficient.

The proposed algorithm diagnoses faulty sensors using the feature points extracted from the sensor outputs based on the cross-error function crossing a defined threshold. Only one such data point is collected every time the sensor output falls into an abnormal region. One or two feature points are not enough to reliably identify the faulty sensors and the corresponding fault characteristics. For systems whose signal changes slowly, it may take a long time to collect a large number of required data points. As a result, it is necessary to know the relationship between the number of feature points

Please cite this article as: C. Lo, et al., Distributed model-based nonlinear sensor fault diagnosis in wireless sensor networks, Mech. Syst. Signal Process. (2015), http://dx.doi.org/10.1016/j.ymssp.2015.05.011

available and the corresponding detection accuracy, especially in identifying the fault pattern in Fig. 7 and estimating the boundaries of the normal regime of a faulty sensor. Two simulation are conducted using the bilinear fault model with θ set to 20° and the exponential model with ψ set to 0.1. Both double-harmonic and white noise excitations are evaluated. As shown in Fig. 13 and as expected, the detection rate and fault region detection rate increase when the number of available feature points increases. The detection rates plateaus when the available feature points reach 10 for the bilinear model and 6 for the exponential model. The result implies that the proposed algorithm is able to detect sensors with non-linear faults using only a small number of feature points (*e.g.*, 10 or more). If a cross-error function always has a large output and the algorithm obtains only a few feature points, it suggests that either the sensor(s) is(are) affected by other type of faults (such as excessive noise) or the dynamics of the structure falls mainly into the non-linear operation region of the sensor(s).

Next, the algorithm performance is evaluated when measurement noise exists in the sensors. The simulation is conducted using the same bilinear fault model with θ set to 30° and the same exponential model with $\psi = 0.1$. Random white Gaussian noise with different noise variance is superimposed to the sensor measurements. The noise variance ratio in Fig. 14 is defined as the ratio of the noise variance to the maximum magnitude of the sensor measurements. As can be seen in Fig. 14, the detection rate decreases as the measurement noise variance increases in both non-linear models. For white-noise excited systems using the bilinear non-linearity model, the fault detection rate is 90% or greater when the noise variance is within 5% of the sensor measurement magnitude. Typical sensor noise is significantly less than 5% for common sensors. Similarly, white-noise excited systems using the exponential model achieved detection rates of 90% or greater under the same noise variance level. As was observed in the previous experiments, the accuracy of the algorithm on double-tone harmonic systems is slightly lower than that of white-noise excited systems. The detection rate on double-tone

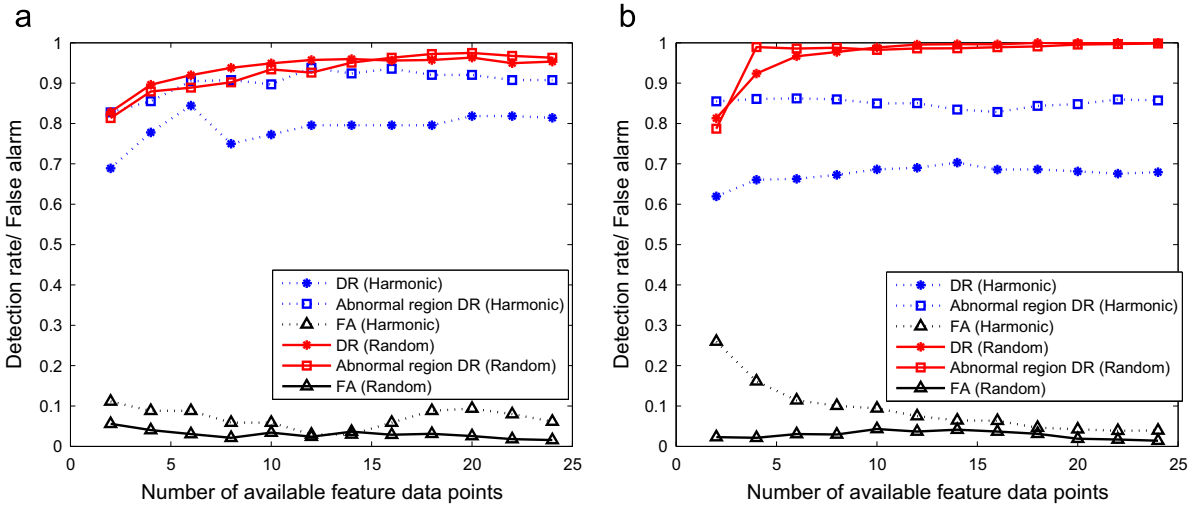

Fig. 13. Detection accuracy versus number of available feature points when using (a) bilinear model and (b) exponential model.

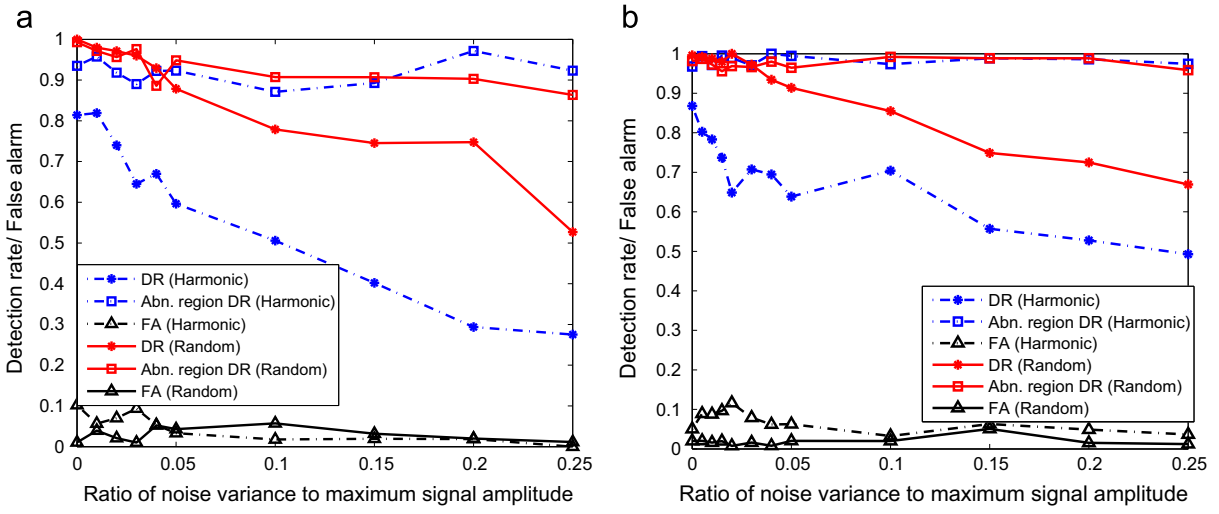

Fig. 14. Detection accuracy versus sensor measurement noise when using (a) bilinear model and (b) exponential model.

Please cite this article as: C. Lo, et al., Distributed model-based nonlinear sensor fault diagnosis in wireless sensor networks, Mech. Syst. Signal Process. (2015), http://dx.doi.org/10.1016/j.ymssp.2015.05.011

harmonic excited systems drops to 60% when the noise variance reaches 5% of the sensor measurement magnitude for bilinear models. For exponential non-linear models, the same detection rate drops to under 60% when the noise variance is larger than 15% of the sensor measurement magnitude. For the abnormal region detection of the correctly detected faulty sensors, the detection rate remains at about 90% of accuracy on different noise variances (for both excitation types and for both non-linear models). This implies the abnormal region detection is less affected by the measurement noise once the faulty sensor is correctly detected.

The influence of the maximum amplitude of the faulty signal relative to boundary, r, is evaluated. Fig. 15 shows the detection rate and false alarm rate as a function of the signal amplitude-normal region boundary (r) ratio for the bilinear and exponential models. The x-axis value is defined as the mean of the maximum sensor output each time the actual signal exceeds the normal region boundary divided by the normal region boundary. As shown in the figure, the fault detection accuracy increases in tandem with the average ratio reaching its maximum when the average ratio is 10% or higher.

As mentioned in Section 3.3, the proposed fault detection algorithm is able to distinguish non-linearity faults from other types of faults by examining the area of the detected largest empty rectangle. This property is illustrated by applying the LER algorithm to sensor data in which $S1$ is corrupted by spike faults, mean drift faults and excessive noise faults, respectively. These faults are common in sensors. Spike faults are sparse impulses superimposed on normal sensor measurements. Mean drift faults preserve the output dynamics but not its mean value. This type of fault generates outputs whose mean drifts away from the true mean of the signal slowly as compared to the output dynamics. Excessive noise refers to a large amount of Gaussian noise in the output of a sensor. The results of the LER algorithm on the sensor data corrupted by these faults are shown in Fig. 16. All the detected LERs have very small areas (compared to the maximum amplitude of the sensor data). This is because the feature points associated with these faults are not always bigger than a fixed boundary. These feature points can locate anywhere in the 2-D plane and thus do not follow any of the patterns in Fig. 7. As a result, non-linearity faults can be distinguished from other types of faults by examining the area of the largest empty rectangle.

5. Conclusion

In this study, a model-based decentralized sensor fault diagnosis algorithm that is designed to target non-linearity faults is proposed. The algorithm is carried out locally within a pair of sensors and thus saves significant amount of data transmission power compared to centralized fault diagnosis methods. This is a crucial characteristic for being able to be applied in power-limited wireless sensor networks. The work verified through simulations that the proposed method is able to identify non-linearity faults accurately. The algorithm generally achieves 90% or greater detection rates and obtains accurate values for the boundaries of the normal region of the non-linearity models. A low-complexity sub-optimal LER algorithm is suggested and is found to have similar performance as the optimal LER algorithm in non-linearity fault detection. The proposed algorithm is able to distinguish the non-linearity faults from the other types of faults. Having the ability to identify fault types is important as it provides information on the fundamental cause of the sensor fault. Also, knowing the fault type helps to recover the corrupted data and thus reduces the sensor replacement cost. Future work includes developing a recovery algorithm which recovers the true signal from the signal corrupted by non-linearity faults. Another possible direction is to develop an identification method for other fault types, such as mean-drift faults, under the same decentralized model-based framework.

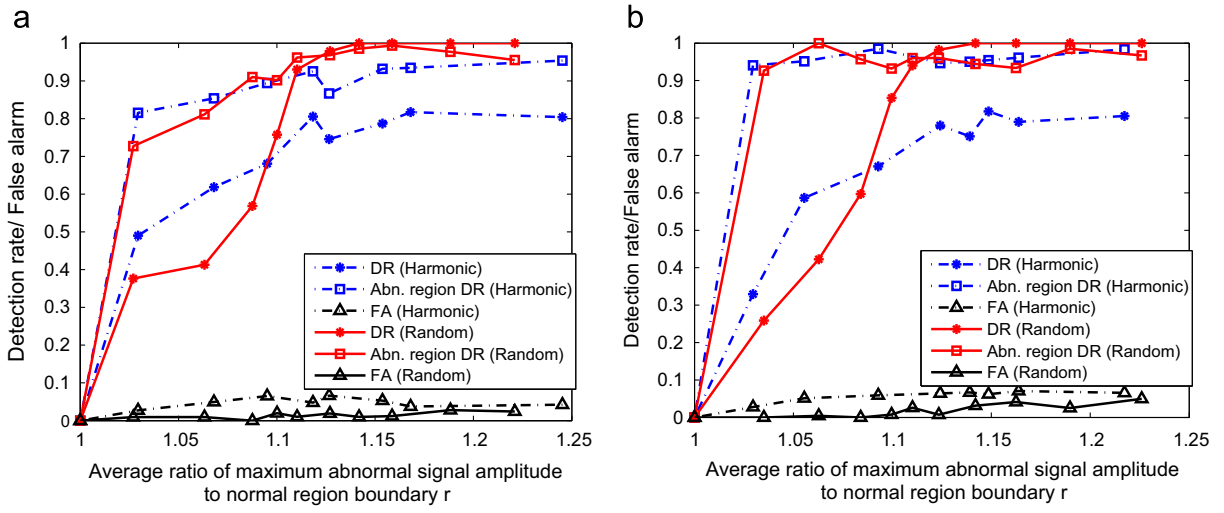

Fig. 15. Detection accuracy versus abnormal signal amplitude when using: (a) bilinear model and (b) exponential model.

Please cite this article as: C. Lo, et al., Distributed model-based nonlinear sensor fault diagnosis in wireless sensor networks, Mech. Syst. Signal Process. (2015), http://dx.doi.org/10.1016/j.ymssp.2015.05.011

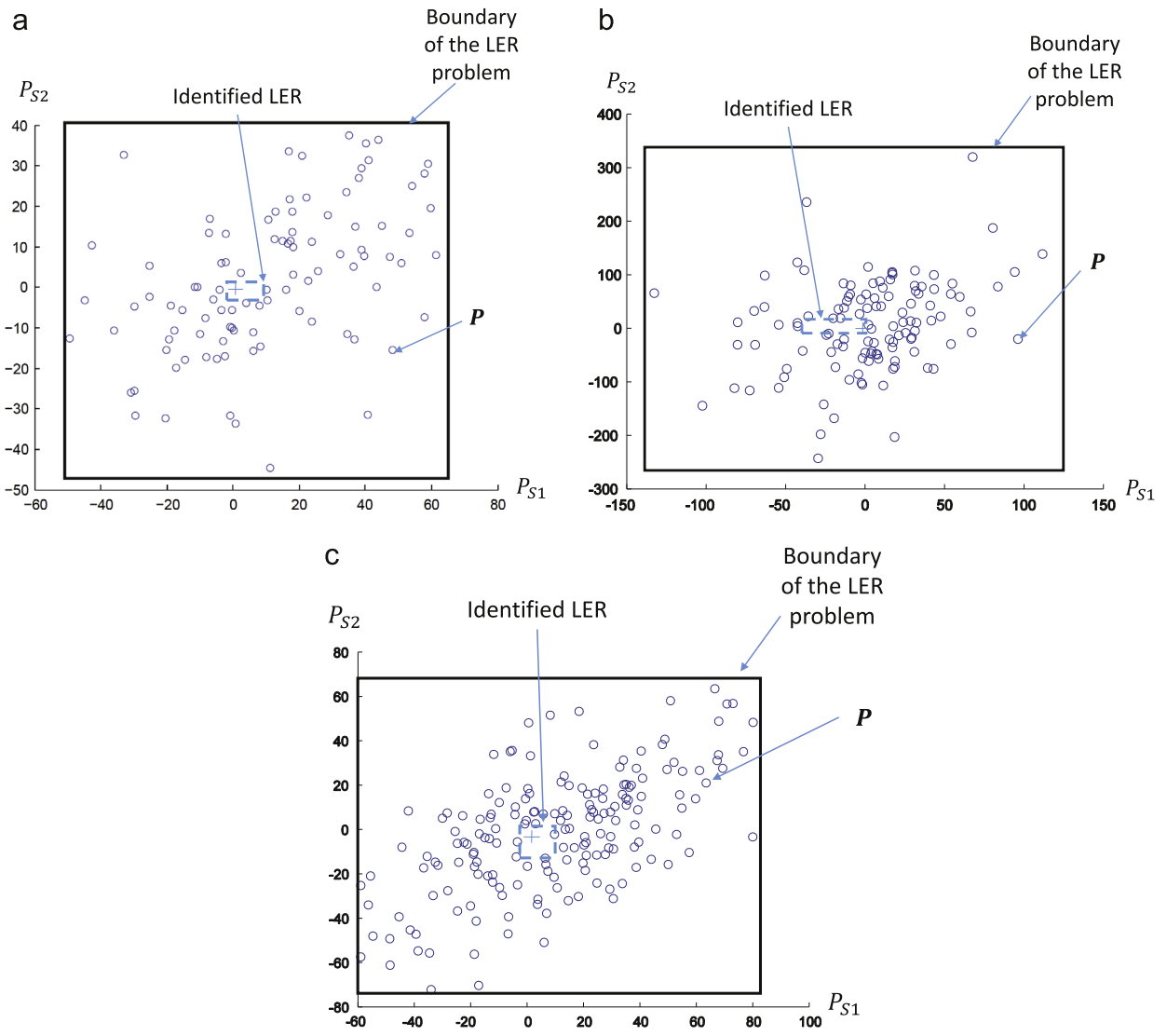

Fig. 16. Illustration of the detected LER when one of the sensors is corrupted by: (a) spike faults, (b) mean-drift faults, and (c) excessive noise faults.

This study assumes that the structure being monitored is healthy throughout the diagnosis period. If the structure is damaged, the cross-error function may exhibit some sensitivity to the structure damage. However, the nature of the system damage may not affect the ability to find nonlinear sensor faults. Specifically, the change of structure characteristics would only affect the sensor fault algorithm if the damage affects the system output when the output is larger than a particular value. Clearly, additional work is needed to explore how structural damage may affect the proposed nonlinear sensor fault method.

Acknowledgements

The authors gratefully acknowledge the generous support provided by the National Science Foundation under Grants CCF-0910765, CMMI-1362513, and ECCS- 1446521. Additional support was provided by the Office of Naval Research under Contracts N00014-09-C0103 and N00014-12-1-0178, and the National Institute of Standards and Technology (NIST) Technology Innovation Program under Cooperative Agreement 70NANB9H9008.

Please cite this article as: C. Lo, et al., Distributed model-based nonlinear sensor fault diagnosis in wireless sensor networks, Mech. Syst. Signal Process. (2015), http://dx.doi.org/10.1016/j.ymssp.2015.05.011

References

[1] J. Lynch, An overview of wireless structural health monitoring for civil structures, Philos. Trans. R. Soc. A: Math., Phys. Eng. Sci. 365 (1851) (2007) 345–372.
[2] T. Wark, P. Corke, P. Sikka, L. Klingbeil, Y. Guo, C. Crossman, P. Valencia, D. Swain, G. Bishop-Hurley, Transforming agriculture through pervasive wireless sensor networks, Pervasive Comput. IEEE 6 (2) (2007) 50–57, http://dx.doi.org/10.1109/MPRV.2007.47.
[3] T. Bokareva, W. Hu, S. Kanhere, B. Ristic, N. Gordon, T. Bessell, M. Rutten, S. Jha, Wireless sensor networks for battlefield surveillance, in: Proceedings of the Land Warfare Conference, 2006.
[4] P. Sikka, P. Corke, L. Overs, Wireless sensor devices for animal tracking and control, in: 29th Annual IEEE International Conference on Local Computer Networks, 2004, pp. 446 – 454, doi:http://dx.doi.org/10.1109/LCN.2004.141.
[5] N. Ramanathan, K. Chang, R. Kapur, L. Girod, E. Kohler, D. Estrin, Sympathy for the sensor network debugger, in: Proceedings of the 3rd International Conference on Embedded Networked Sensor Systems, SenSys'05, ACM, New York, NY, USA, 2005, pp. 255–267.
[6] L. Ruiz, I. Siqueira, L. e. Oliveira, H. Wong, J. Nogueira, A. Loureiro, Fault management in event-driven wireless sensor networks, in: Proceedings of the 7th ACM International Symposium on Modeling, Analysis and Simulation of Wireless and Mobile Systems, MSWiM'04, ACM, New York, USA, 2004, pp. 149–156.
[7] M. Goodrich, D. Hirschberg, Efficient parallel algorithms for dead sensor diagnosis and multiple access channels, in: Proceedings of the Eighteenth Annual ACM Symposium on Parallelism in Algorithms and Architectures, ACM, Cambridge, MA, 2006, pp. 118–127.
[8] E. Chow, A. Willsky, Analytical redundancy and the design of robust failure detection systems, IEEE Trans. Autom. Control 29 (7) (1984) 603–614.
[9] R. Da, C. Lin, Sensor failure detection with a bank of kalman filters, in: Proceedings of the American Control Conference, vol. 2, IEEE, Seattle, WA, 1995, pp. 1122–1126.
[10] T. Kobayashi, D. Simon, Application of a Bank of Kalman Filters for Aircraft Engine Fault Diagnostics, Technical Report, DTIC Document, 2003.
[11] V. Ricquebourg, D. Menga, M. Delafosse, B. Marhic, L. Delahoche, A. Jolly-Desodt, Sensor failure detection within the tbm framework: a Markov chain approach, in: Proceedings of the IPMU, vol. 8, 1991, p. 323.
[12] X. Xu, J. Hines, R. Uhrig, Sensor validation and fault detection using neural networks, in: Proceedings of the Maintenance and Reliability Conference (MARCON 99), Citeseer, 1999, pp. 10–12.
[13] R. Dunia, S. Qin, T. Edgar, T. McAvoy, Identification of faulty sensors using principal component analysis, AIChE J. 42 (10) (2004) 2797–2812.
[14] G. Kerschen, J. De Boe, P. Golinval, K. Worden, Sensor validation using principal component analysis, Smart Mater. Struct. 14 (1) (2005) 36.
[15] J. Chen, S. Kher, A. Somani, Distributed fault detection of wireless sensor networks, in: Proceedings of the 2006 Workshop on Dependability Issues in Wireless Ad Hoc Networks and Sensor Networks, ACM, Los Angeles, CA, 2006, pp. 65–72.
[16] S. Guo, Z. Zhong, T. He, Find: faulty node detection for wireless sensor networks, in: Proceedings of the 7th ACM Conference on Embedded Networked Sensor Systems, ACM, Berkeley, CA, 2009, pp. 253–266.
[17] M. Ding, D. Chen, K. Xing, X. Cheng, Localized fault-tolerant event boundary detection in sensor networks, in: Proceedings of the 24th Annual Joint Conference of the IEEE Computer and Communications Societies, INFOCOM 2005, vol. 2, IEEE, Miami, FL, 2005, pp. 902–913, http://dx.doi.org/10.1109/INFCOM.2005.1498320.
[18] X. Luo, M. Dong, Y. Huang, On distributed fault-tolerant detection in wireless sensor networks, IEEE Trans. Comput. 55 (1) (2006) 58–70.
[19] G. Gautschi, Piezoelectric Sensorics: Force, Strain, Pressure, Acceleration and Acoustic Emission Sensors, Materials and Amplifiers, Springer, New York, NY, 2002.
[20] R. Tokars, J. Lekki, Self diagnostic accelerometer ground testing on a c-17 aircraft engine, in: Aerospace Conference, IEEE, Big Sky, MT, 2013, pp. 1–8.
[21] J. Fraden, Handbook of Modern Sensors, Springer, 2010.
[22] C. Lo, J. Lynch, M. Liu, Distributed reference-free fault detection method for autonomous wireless sensor networks, Sens. J. IEEE 13 (5) (2013) 2009–2019, http://dx.doi.org/10.1109/JSEN.2013.2244881.
[23] L. Lennart, System Identification: Theory for the User, PTR Prentice Hall, Upper Saddle River, NJ.
[24] J. Lynch, A. Sundararajan, K. Law, A. Kiremidjian, E. Carryer, Embedding damage detection algorithms in a wireless sensing unit for operational power efficiency, Smart Mater. Struct. 13 (2004) 800.
[25] Y. Monden, M. Yamada, S. Arimoto, Fast algorithm for identification of an arx model and its order determination, IEEE Trans. Acoust. Speech Signal Process. 30 (3) (1982) 390–399.
[26] H. Kaplan, M. Sharir, Finding the Maximal Empty Rectangle Containing a Query Point, arXiv preprint arXiv:1106.3628.
[27] G. Gutiérrez, J. Paramá, Finding the Largest Empty Rectangle Containing Only a Query Point in Large Multidimensional Databases, Scientific and Statistical Database Management, Springer, New York, NY, 2012, 316–333.
[28] S. Nandy, B. Bhattacharya, S. Ray, Efficient Algorithms for Identifying All Maximal Isothetic Empty Rectangles in vlsi Layout Design, Foundations of Software Technology and Theoretical Computer Science, Springer, New York, NY, 1990, 255–269.
[29] R. Tarjan, Efficiency of a good but not linear set union algorithm, J. ACM 22 (2) (1975) 215–225.
[30] Z. Li, B. Koh, S. Nagarajaiah, Detecting sensor failure via decoupled error function and inverse input–output model, J. Eng. Mech. 133 (11) (2007) 1222–1228.

Please cite this article as: C. Lo, et al., Distributed model-based nonlinear sensor fault diagnosis in wireless sensor networks, Mech. Syst. Signal Process. (2015), http://dx.doi.org/10.1016/j.ymssp.2015.05.011